Robust Landing Stabilization of Humanoid Robot on Uneven Terrain via Admittance Control and Heel Strike Motion

Joonhee Jo[1,2], Gyunghoon Park[3], and Yonghwan Oh[1]

***Abstract*— This paper addresses robust landing stabilization in humanoid locomotion on uneven terrain. The core idea is to find a configuration of the robot that results in small impulsive force when an unexpected obstacle is encountered, and to adjust post-contact reference for swing foot with which the pose of the foot is stabilized on the obstacle. This can be achieved by walking with heel strike motion (validated by the impact map analysis) and by employing hybrid admittance control combining the admittance control with reset of post-contact reference, embedded into the momentum-based whole-body control framework. The validity of the proposed algorithm is verified by simulation with a physics engine.**

I. Introduction

The humanoid locomotion is the primary interaction with the ground, considering the reaction forces. The balancing control of the robot can be obtained when the ground contact force is properly controlled. The problem of balance control arises critically when the robot walks on rough terrain whose height and altitude vary, which affects the robot's stability.

For stable walking in such uncertain environments, stabilization of swing foot even in the presence of obstacles, termed as "(robust) landing stabilization" in this paper, is studied in several directions. To resolve the impact energy on the robot, [1] has approached the problem by passivity theory, or [2]–[4] augmented a virtual spring-damper in-between hip and ankle joints, at the ankle, and at the foot. Meanwhile, the concept of impedance control [5] and admittance control [6]–[8] are applied into the humanoid robot landing and balancing control.

The aforementioned researches have dealt with the contact force control problem at the moment of contact. On the other hand, some researchers tried to mimic the human motion because the human walks with the heel strike motion to improve the walking efficiency and dissipate the impact [9]. Robotics researchers tried the heel strike walking by generating the trajectory following the gait cycle [10] and optimization [11]. By specifying the desired touchdown angle, heel strike behavior can be obtained [12] with momentum-based whole-body control [13].

At first, a momentum-based torque control scheme might ensure robustness in uneven terrain locomotion however, in some cases, it fails to landing task and lose the balance because of the unexpected contact force. To resolve the issue, this paper proposes two strategies for landing stabilization that enhance robustness of momentum-based whole-body control framework. First, a combination of the admittance control and reset strategy (called "hybrid admittance control (**HAC**)" throughout this paper) is embedded into the momentum-based whole-body control framework to stabilize the constrained and unconstrained motions of landing foot simultaneously. In addition, it is revealed via impact map analysis in terms of impulsive force that a pre-contact motion with heel strike could help to robustly stabilize the landing task. This finding is in fact supported by some results on the human locomotion [9], yet not many attention has been paid in the robotics literature to use the heel strike motion for landing stabilization on uneven terrain. To show the validity of the proposed algorithm, a set of simulations with a physics engine is performed, revealing that the proposed method significantly improves the robustness of the momentum-based whole-body control framework in landing stabilization tasks.

The rest of this paper is organized as follows. Subsection II-A first revisits a momentum-based whole-body control framework and a robot model for its introduction. The proposed landing control law will be embedded in the upcoming sections. After that, in subsection II-B, the importance and difficulties of stable landing are highlighted. In addition, robust landing stabilization with the pre-contact strategy in section III, and **HAC** in section IV. The experimental results are followed and discussed in section V.

II. Problem Statement

This paper aims to present a compliant landing control of a humanoid robot that walks on uneven terrain, as depicted in Fig. 1.

A. Momentum based whole-body control

The equations of motion (EoM) of the robot system described in Fig. 1 are expressed as

$$\underbrace{\begin{bmatrix}\boldsymbol{M}_B\\ \boldsymbol{M}_q\end{bmatrix}}_{\boldsymbol{M}}\ddot{\boldsymbol{\xi}}+\underbrace{\begin{bmatrix}\boldsymbol{C}_B\\ \boldsymbol{C}_q\end{bmatrix}}_{\boldsymbol{C}}\dot{\boldsymbol{\xi}}+\underbrace{\begin{bmatrix}\boldsymbol{g}_B\\ \boldsymbol{g}_q\end{bmatrix}}_{\boldsymbol{g}}=\underbrace{\begin{bmatrix}\boldsymbol{0}\\ \boldsymbol{B}_q\end{bmatrix}}_{\boldsymbol{B}}\boldsymbol{\tau}+\sum_{k\in N_e}\underbrace{\begin{bmatrix}\boldsymbol{X}_{t_kB}^T\\ \hat{\boldsymbol{J}}_{t_k}^T\end{bmatrix}}_{\boldsymbol{\Phi}_{t_k}^T}\boldsymbol{\lambda}_{C_k} \quad (1)$$

where $\dot{\boldsymbol{\xi}} = \begin{pmatrix}\dot{\boldsymbol{x}}_B^T & \dot{\boldsymbol{q}}^T\end{pmatrix}^T \in \Re^{n+6}$ and $\ddot{\boldsymbol{\xi}} \in \Re^{n+6}$ are the generalized coordinates velocity and the acceleration, respectively, and $N_e := \{r, l\}$. $\boldsymbol{M}, \boldsymbol{C} \in \Re^{(n+6)\times(n+6)}$ are an inertia matrix and a Coriolis and Centrifugal matrices of the body and $\boldsymbol{g} \in \Re^{(n+6)}$ is a gravitational force vector.

[1]J. Jo and Y. Oh are with Center for Intelligent & Interactive Robotics, Korea Institute of Science and Technology (KIST), Seoul, 136-791, Korea (email: jhjo@kist.re.kr and oyh@kist.re.kr)

[2]J. Jo is with Department of HCI & Robotics, University of Science and Technology(UST), Daejeon, 305-350, Korea

[3]G. Park is with School of Electrical and Computer Engineering, University of Seoul, 163, Seoulsiripdaero, Dongdaemun-gu, Seoul 02504, Korea (email: gyunghoon.park@uos.ac.kr)

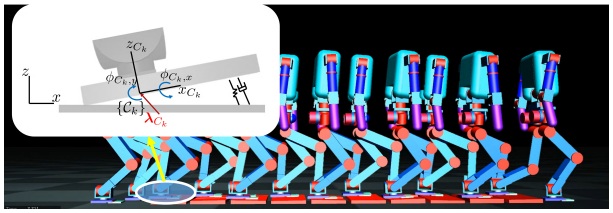

Fig. 1: A humanoid locomotion system on uneven terrain.

$\boldsymbol{B} \in \Re^{(n+6)\times n}$ is a constant selection matrix. $\boldsymbol{X}_{t_k B}, \hat{\boldsymbol{J}}_{t_k}$ are parts of Jacobian related to the velocity of the body and the joint. $\boldsymbol{\lambda}_{C_k} = \begin{pmatrix} \boldsymbol{f}_{C_k}^T & \boldsymbol{\mu}_{C_k}^T \end{pmatrix}^T \in \Re^6$ is the contact force vector and $\boldsymbol{\tau}$ is joint torque. Throughout this paper, $\boldsymbol{\lambda}_{C_k}$ is abbreviated as $\boldsymbol{\lambda}_k$ for simplicity.

The QP-based torque control has been widely employed as a useful tool for achieving control tasks and handling the redundancy of the robot [14]. A conventional form of this control law is given by

$$\begin{aligned} \boldsymbol{z}^* \;=\; & \underset{\boldsymbol{z}}{\operatorname{argmin}} \frac{1}{2} \left\| \boldsymbol{A}_{ob}\boldsymbol{z} - \boldsymbol{b}_{ob} \right\|_{\boldsymbol{W}_1}^2 + \frac{1}{2} \left\| \boldsymbol{z} \right\|_{\boldsymbol{W}_2}^2 \\ & \text{s.t.} \quad \boldsymbol{A}_{ec}\boldsymbol{z} = \boldsymbol{b}_{ec},\ \boldsymbol{A}_{ic}\boldsymbol{z} \le \boldsymbol{b}_{ic},\ \boldsymbol{z}_{min} \le \boldsymbol{z} \le \boldsymbol{z}_{max} \end{aligned} \tag{2}$$

where $\boldsymbol{z} = \begin{pmatrix} \ddot{\boldsymbol{\xi}}^T & \boldsymbol{\beta}_k^T \end{pmatrix}^T$ is the decision variable of (2) while the force intensities $\boldsymbol{\beta}_k$ is defined to satisfy $\boldsymbol{\lambda}_k = \boldsymbol{U}_k\boldsymbol{\beta}_k$ with a basis matrix $\boldsymbol{U}_k$, and $\boldsymbol{W}_1$ and $\boldsymbol{W}_2$ are weighting matrices. The matrices and vectors in (2) characterize the task/objective $(\boldsymbol{A}_{ob}, \boldsymbol{b}_{ob})$, equality constraints $(\boldsymbol{A}_{ec}, \boldsymbol{b}_{ec})$, inequality constraints $(\boldsymbol{A}_{ic}, \boldsymbol{b}_{ic})$, and additional bounds $(\boldsymbol{z}_{min}, \boldsymbol{z}_{max})$. The objective function of (2) is set to achieve the tracking control of the centroidal momentum, body orientation, and end-effectors such as swing foot, trunk, and arms. Meanwhile, the equality/inequality constraints are added to keep (1) and contact acceleration constraint, joint angle limit, and friction cone approximation [15].

The QP (2) is solved to find the optimal solution $\boldsymbol{z}^*$ as a control input to compute the command torque (1):

$$\boldsymbol{\tau}_C = \boldsymbol{M}_q\ddot{\boldsymbol{\xi}}^* + \boldsymbol{C}_q\dot{\boldsymbol{\xi}} + \boldsymbol{g}_q - \sum_{k\in N_e} \boldsymbol{J}_{t_k}^T \boldsymbol{\lambda}_k^* \tag{3}$$

where $\boldsymbol{\lambda}_k^* = \boldsymbol{U}_k\boldsymbol{\beta}_k^*$.

B. Stable landing on uneven terrain

The walking task is achieved by moving the frame of the swing foot $\boldsymbol{x}_{t_k}$ to track its desired trajectory $\boldsymbol{x}_{t_k,d}^*$. Hereinafter, the subscript t_k which stands for the "k-th task" is dropped for simplicity so $\boldsymbol{x}_{t_k}, \boldsymbol{x}_{t_k,d}^*$ are abbreviated as $\boldsymbol{x}, \boldsymbol{x}_d^*$.

The k-th task motion at the contact position is described from the direct kinematics $\mathcal{K} : \Re^n \to \Re^6$ which is mapping from the generalized coordinates $\boldsymbol{\xi}$, $\boldsymbol{x} = \mathcal{K}(\boldsymbol{\xi})$. In addition, the task velocity is $\dot{\boldsymbol{x}} = \boldsymbol{\Phi}\dot{\boldsymbol{\xi}}$ and task acceleration $\ddot{\boldsymbol{x}} = \boldsymbol{\Phi}\ddot{\boldsymbol{\xi}} + \dot{\boldsymbol{\Phi}}\dot{\boldsymbol{\xi}}$. In the QP-based torque control framework, the walking task can be done by adding $\left\| \ddot{\boldsymbol{x}} - \ddot{\boldsymbol{x}}_r^* \right\|_{\boldsymbol{W}}^2$ with

$$\ddot{\boldsymbol{x}}_r = \ddot{\boldsymbol{x}}_d + \boldsymbol{K}_v\left(\dot{\boldsymbol{x}}_d - \dot{\boldsymbol{x}}\right) + \boldsymbol{K}_p\left(\boldsymbol{x}_d - \boldsymbol{x}\right) \tag{4}$$

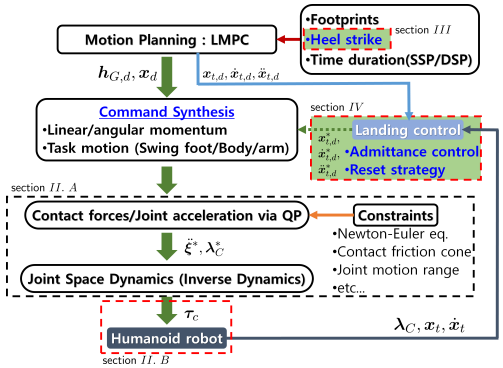

Fig. 2: The block diagram of the overall control framework. The proposed algorithms are highlighted as dotted blocks.

to the objective function of the QP in (2), where $\boldsymbol{K}_v$ and $\boldsymbol{K}_p$ are control gain matrices for damping and stiffness, respectively.

To continue walking steadily, it is also necessary to regulate the tracking error $\boldsymbol{x} - \boldsymbol{x}_d$ and $\dot{\boldsymbol{x}} - \dot{\boldsymbol{x}}_d$ quickly within a finite time before the next swing phase begins. This substantial task is referred to as "stable landing" in this paper. Achieving stable landing during the walking is challenging, especially when the robot encounters uneven terrain, resulting in an undesired contact with the ground at a later or earlier moment than expected. At first glance, the late contact may be dealt with by the QP-based torque control, relying on its inherent compliance and the so-called gliding behavior due to the zero-contact acceleration condition (i.e., $\ddot{\boldsymbol{x}} = 0$) added to a constraint of (2) during the stance phase. However, when it comes to the early contact case, stable landing is not that straightforward by only using the QP-based torque control. The main difficulty is that, at the moment of an early contact, a non-zero tracking error $\boldsymbol{x} - \boldsymbol{x}_d$ generates an unnecessary contact space force, by which the balance of the robot may be lost. To clarify this point, consider the moment balance with respect to the inertial frame

$$\begin{aligned} \boldsymbol{\mu}_o \;&=\; \sum_k \left[\left(\boldsymbol{p}_G - \boldsymbol{p}_{C_k} \right) \times \boldsymbol{f}_k + \boldsymbol{\mu}_k \right] \\ &=\; \dot{\boldsymbol{k}}_G + \left(\boldsymbol{p}_G - \boldsymbol{p}_{ZMP} \right) \times m_G \left(\ddot{\boldsymbol{p}}_G + \bar{\boldsymbol{g}} \right) \end{aligned} \tag{5}$$

where $\dot{\boldsymbol{k}}_G$ is the rate of angular momentum, and $\boldsymbol{p}_{C_k}$ is k-th contact position. $\boldsymbol{p}_G, \ddot{\boldsymbol{p}}_G$ and $\boldsymbol{p}_{ZMP}$ are the position and the acceleration of the center of mass (CoM), respectively, and the zero moment point (ZMP). m_G and $\bar{\boldsymbol{g}}$ are the robot mass and the gravity vector. Then it is readily seen in (5) that the unexpected contact force $\boldsymbol{\lambda}_k$ (whose quantity becomes larger as the control gain used gets higher) possibly leads to large perturbations of $\dot{\boldsymbol{k}}_G$, $\boldsymbol{p}_G$, $\ddot{\boldsymbol{p}}_G$, and $\boldsymbol{p}_{ZMP}$ so that some requirements for the balance turn out to be violated. This might be handled simply by lowering the control gain however such approach has a limitation because the tracking performance is sacrificed.

In this regard, this paper proposes two strategies to achieve stable landing on uneven terrain: 1) finding a "good" can-

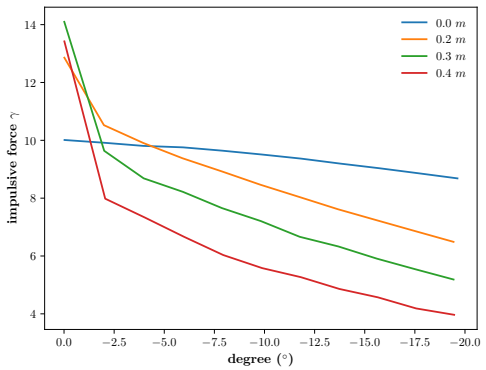

Fig. 3: Impact experiment result with heel strikes w.r.t. various step strides. The legend denotes the step stride of the humanoid and the angle in x-axis is the heel strike angle, and impulsive force is in y-axis.

didate for the desired trajectory $\boldsymbol{x}^*_{C_k,d}$ that results in a moderate amount of the impact when the foot contacts the ground earlier (pre-landing strategy), and 2) adjusting the trajectory during the landing phase to reduce the effect of the unexpected impact after the contact (post-landing strategy). For the implementation of this idea, heel strike landing and admittance-based control with reset strategy play a central role. (Throughout this paper, the latter is termed a "hybrid landing control" to emphasize its hybrid nature.) The overall configuration of the closed-loop system with the proposed algorithm is described in Fig. 2.

III. Pre-contact strategy via heel strike walking

The literature on human locomotion has reported that, non-zero angle of the heel strike is often beneficial in walking, especially for minimization of energy consumption [16], [17]. Motivated by this, but from a different point of view, this section reveals that the swing foot's heel strike motion significantly reduces the impulsive force generated by an unexpected contact.

For the analysis to come, an explicit form of the impulsive force is carried out first. It is noted in advance that the impact analysis via the impulsive force has been conducted mostly for manipulators [18], [19], while our study will reach a different conclusion as the base and configuration of the humanoid are not the same as those of the manipulators. Consider the task space dynamics of the foot

$$\boldsymbol{\lambda} = \boldsymbol{M}_x\ddot{\boldsymbol{x}} + \boldsymbol{C}_x\dot{\boldsymbol{x}} + \boldsymbol{g}_x \tag{6}$$

where $\boldsymbol{\lambda}$ is the contact force. In addition, $\boldsymbol{M}_x$, $\boldsymbol{C}_x$, and $\boldsymbol{g}_x$ are the task space inertia, Coriolis & Centrifugal term, and gravity. In what follows, the impact at the contact with the ground is assumed to last for an infinitesimally short time period. Taking an integration of (6) with a small period of time, the following relations are obtained:

$$\begin{aligned} \Delta\boldsymbol{\lambda} &= \lim_{\Delta t\to 0}\int_t^{t+\Delta t}\boldsymbol{\lambda}(s)ds \\ &= \lim_{\Delta t\to 0}\boldsymbol{M}_x\left(\dot{\boldsymbol{x}}(t+\Delta t)-\dot{\boldsymbol{x}}(t)\right) = \boldsymbol{M}_x\Delta\dot{\boldsymbol{x}} \end{aligned} \tag{7}$$

where $\Delta\boldsymbol{\lambda} = \gamma\boldsymbol{n}_C$ is the impulsive force with the magnitude γ and the normal vector $\boldsymbol{n}_C$ to the contact surface. Assuming the rigid body collision, the pre- and post-impact velocities are related as

$$\left(\dot{\boldsymbol{x}}+\Delta\dot{\boldsymbol{x}}\right)^T\boldsymbol{n}_C = -e\dot{\boldsymbol{x}}_C^T\boldsymbol{n}_C \tag{8}$$

where e is the restitution parameter that characterizes the collision type. Finally, for a comparison of configurations independently of $\|\dot{\boldsymbol{x}}\|$, the impulsive force is computed by substituting (7) into (8) and by normalizing $\dot{\boldsymbol{x}}$ as follows:

$$\gamma = -\frac{(1+e)\left(\dot{\boldsymbol{x}}/\|\dot{\boldsymbol{x}}\|\right)^T\boldsymbol{n}_C}{\boldsymbol{n}_C^T\boldsymbol{M}_x^{-1}\boldsymbol{n}_C} \tag{9}$$

where $\boldsymbol{M}_x^{-1} = \boldsymbol{\Phi}\boldsymbol{M}^{-1}\boldsymbol{\Phi}^T$ and $e = 0$ for the plastic case.

To exploit the relation between the impulsive force and the configuration, a set of simulations are performed for a humanoid robot walking on flat ground, with different heel strike angles (from $0°$ to $18°$) and different step strides (from $0\ m$ to $0.4\ m$). (For the simulation, the humanoid model in Fig. 1 is used, whose details will be presented shortly.) The simulation result given in Fig. 3 shows that the magnitude γ in (9) of the normalized impulsive force is decreased as the heel strike angle is increased, regardless of the stride length.

While the impact analysis above suggests to take the heel strike angle as large as possible for small impulsive force, this may not be possible when other physical constraints need to be met. With this trade-off in mind, a heel strike angle within the range of $0° \sim 5°$ is employed in the design of $\boldsymbol{x}^*_d$, taking step length and uncertainty of terrain into account and being backed by the existing works on the human locomotion [16], [17].

It is also important to note that, from (7), the velocity change as a result of the impact becomes

$$\Delta\dot{\boldsymbol{x}} = \boldsymbol{M}_x^{-1}\Delta\boldsymbol{\lambda} = \left(\boldsymbol{\Phi}\boldsymbol{M}^{-1}\boldsymbol{\Phi}^T\right)\Delta\boldsymbol{\lambda}. \tag{10}$$

This highlights that heel strike motion of the swing foot (which leads to a smaller $\Delta\boldsymbol{\lambda}_C$) could outperform the flat foot motion in the landing stabilization, where the foot velocity needs to be regulated rapidly after a contact.

IV. Post-contact strategy via hybrid admittance control

Because the foot is constrained in the contact space $\{\mathcal{C}\}$, undesired foot motion is possibly led by a contact force at the moment of contact, mostly in the perpendicular direction to the contact surface. This motivates us to categorize the 6 axes of the foot frame into two groups: 3 of them (position in z-axis and orientation in x- and y-axes) are related to the constrained motion. Simultaneously, the remaining ones (position in x- and y-axes and orientation in z-axis) are to the unconstrained motion. In this section, the former is called

landing-related axes, while the latter is slip-related axes. Based on such a characterization, two control strategies are proposed according to the considered axes whose combined form is termed as **HAC**. The objective of the **HAC** is handling 1) the constrained motion in the landing-related axes by the admittance control to regulate the foot velocity fast, and 2) the unconstrained motion in the slip-related axes by a reset strategy to keep staying on the contact point.

From the unexpected contact at the swing foot, the modified acceleration reference used in (2) can be obtained from the error dynamics as

$$\begin{aligned} \ddot{\boldsymbol{x}}_r = \ddot{\boldsymbol{x}}_d^* &+ \boldsymbol{K}_v\left(\dot{\boldsymbol{x}}_d^* - \dot{\boldsymbol{x}}\right) + \boldsymbol{K}_p\left(\boldsymbol{x}_d^* - \boldsymbol{x}\right) \qquad (11) \\ \text{where} \quad \boldsymbol{x}_d^* &= \boldsymbol{x}_d + \boldsymbol{x}_l + \boldsymbol{x}_s \\ \dot{\boldsymbol{x}}_d^* &= \dot{\boldsymbol{x}}_d + \dot{\boldsymbol{x}}_l + \dot{\boldsymbol{x}}_s \\ \ddot{\boldsymbol{x}}_d^* &= \ddot{\boldsymbol{x}}_d + \ddot{\boldsymbol{x}}_l + \ddot{\boldsymbol{x}}_s \end{aligned}$$

where $\boldsymbol{x}_d, \dot{\boldsymbol{x}}_d, \ddot{\boldsymbol{x}}_d \in \Re^6$ are the desired position/orientation, velocity, acceleration. $\boldsymbol{x}_d^*, \dot{\boldsymbol{x}}_d^*, \ddot{\boldsymbol{x}}_d^*, \in \Re^6$ are the modified trajectories. $\boldsymbol{x}_l, \dot{\boldsymbol{x}}_l, \ddot{\boldsymbol{v}}_l \in \Re^6$ are landing-related adjustment vectors derived in Subsection IV-A and $\boldsymbol{x}_s, \dot{\boldsymbol{x}}_s, \ddot{\boldsymbol{x}}_s \in \Re^6$ are slip-related reset vectors described in Subsection IV-B.

A. Stabilization of landing-related motion via admittance control

First, to stabilize the landing-related motion, the admittance control is adopted as a tool for modifying the reference trajectory $\boldsymbol{x}_d$. From the unexpected contact force, the desired impedance of the foot system with respect to $\{\mathcal{C}\}$ described in Fig. 1 becomes

$$\boldsymbol{M}_d\left({}^c\ddot{\boldsymbol{s}}_l - {}^c\ddot{\boldsymbol{s}}_{l,d}\right) + \boldsymbol{B}_d\left({}^c\dot{\boldsymbol{s}}_l - {}^c\dot{\boldsymbol{s}}_{l,d}\right) + \boldsymbol{K}_d\left({}^c\boldsymbol{s}_l - {}^c\boldsymbol{s}_{l,d}\right) = \boldsymbol{P}_l^T {}^c\boldsymbol{\lambda}_C \qquad (12)$$

where $\boldsymbol{M}_d, \boldsymbol{B}_d, \boldsymbol{K}_d \in \Re^{3\times3}$ are control gain matrices for mass, damping, and stiffness, respectively, which is designed using DOE. In addition, $\boldsymbol{P}_l \in \Re^{6\times3}$ are selection matrix for landing related axes. ${}^c\boldsymbol{s}_l = \begin{pmatrix} z & \phi_x & \phi_y \end{pmatrix}^T$ is the landing related vector with respect to $\{\mathcal{C}\}$, and ${}^c\dot{\boldsymbol{s}}_l, {}^c\ddot{\boldsymbol{s}}_l$ are its first and second derivatives. $\boldsymbol{s}_{l,d}, \dot{\boldsymbol{s}}_{l,d}, \ddot{\boldsymbol{s}}_{l,d}$ are the desired trajectories for landing related axes, and $\boldsymbol{\lambda}_C$ is the contact force. Using contact space impedance (12), adjustment motion is obtained by admittance relation

$${}^c\ddot{\boldsymbol{e}}_l = \boldsymbol{M}_d^{-1}\left(\boldsymbol{P}_L^T {}^c\boldsymbol{\lambda}_C - \boldsymbol{B}_d({}^c\dot{\boldsymbol{s}} - {}^c\dot{\boldsymbol{s}}_d) - \boldsymbol{K}_d({}^c\boldsymbol{s} - {}^c\boldsymbol{s}_d)\right) \qquad (13)$$

where $\ddot{\boldsymbol{e}}_l \in \Re^3$ is the adjustment acceleration for the landing related axes. The adjustment trajectory $\boldsymbol{e}_l$ and velocity $\dot{\boldsymbol{e}}_l$ can be obtained by the time integration. In the absence of contact, the admittance control is equivalent to the original motion task. Finally, the adjustment trajectory becomes $\ddot{\boldsymbol{x}}_l = \boldsymbol{R}_c\boldsymbol{P}_l{}^c\ddot{\boldsymbol{e}}_l$. $\boldsymbol{x}_l, \dot{\boldsymbol{x}}_l$ are obtained in the same manner. The adjustment vectors are used to modify the desired trajectories.

B. Slip-free motion with reset strategy

When the contact takes place, the desired trajectory $\boldsymbol{x}_d$ in the slip-related axes should be re-assigned. This is mainly because, as depicted in Fig. 4, non-zero tracking error in the slip-related axes drives the robot's swing foot to move to the original target point (which however cannot be reached because of unexpected obstacle on the ground), possibly leading to a slip motion of the foot. A remedy for tackling the issue is to reset the desired pose ${}^c\boldsymbol{s}_s = \begin{pmatrix} x & y & \phi_z \end{pmatrix}^T$ in the slip-related axes with respect to $\{\mathcal{C}\}$, so that such an unnecessary tracking error will be vanished and no slip motion will be generated. $\boldsymbol{P}_s \in \Re^{6\times3}$ are selection matrix for slip related axes. For this purpose, the slip-related adjustment vector is designed as $\boldsymbol{x}_s = \boldsymbol{R}_c\left(\boldsymbol{P}_s{}^c\boldsymbol{s}_s - \boldsymbol{P}_s\boldsymbol{P}_s^T{}^c\boldsymbol{x}_d\right)$ and its derivatives, where $\boldsymbol{x}_s$ is the contact position of the swing foot in the slip-related axes at the moment of contact, which is a constant value.

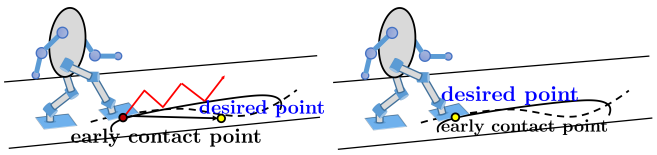

(a) Early contact before reset. (b) Early contact after reset.

Fig. 4: Illustration of early contact case with/without the reset strategy. The black dashed line is the desired trajectory of the foot. The red point is the contact position, and the yellow point is the desired position.

V. Simulation

As described in Fig. 1, the humanoid model has 67.2kg of weight, including 26.2kg for the body, 14.5kg for each leg, and 6Kg for each arm. The robot has 28 DoF with 22 joints (6 for each leg, 2 for the trunk, 4 for each arm). The body motion $\dot{\boldsymbol{p}}_B, \boldsymbol{\omega}_B$ are given from the simulator. The simulation is performed using dynamics engine **MuJoCo** [20]. The control algorithms are written in C++ in Visual Studio, and the simulation is conducted with a 2kHz sampling rate and the 1kHz control rate.

As a validation process, the simulation is performed with/without the proposed algorithm. Every simulation in this paper has been run with the given x-direction walking pattern assumed with the plane ground, 0.30m of step size, 1.5s of one step (1.2s for single support phase, 0.3s for double support phase). In addition, FT sensor has been mounted below the ankle, so the robot leg's movement generates small forces due to the foot dynamics. To tackle this issue, the force threshold hold is set. Additionally, the value of the modified reference is initialized in each supporting state to avoid abusing the integration.

A. Heel strike walking analysis

To see the effect of pre-impact strategy, the comparison between the heel strike and the flat foot walking on uneven terrain locomotion is conducted concerning the velocity change and the impulsive force, as shown in Fig. 5. The 1cm of obstacle induces the early contact in the middle of the footpath. $\dot{\boldsymbol{z}}_d, \dot{\boldsymbol{z}}_{d2}$ refer to the desired flat foot and heel strike trajectory. **FF** and **HS** refer to the flat foot and the heel strike trajectory. The early contact occurs at $8.97s$ for flat foot and $8.91s$ for heel strike. As described in section III, the velocity change of **HS** is smaller than **FF** after the

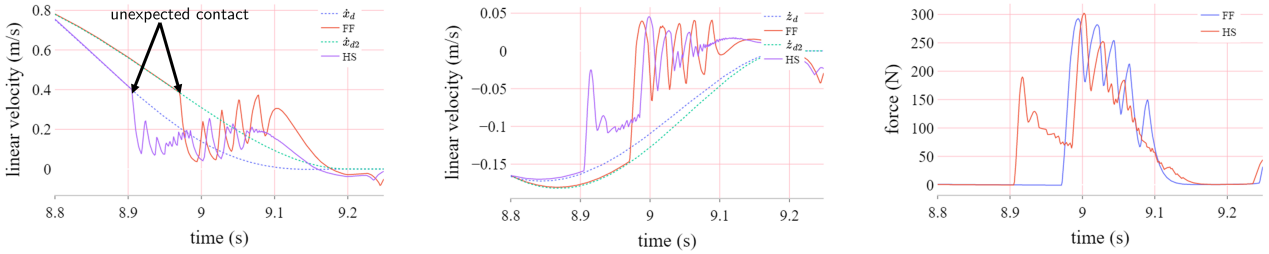

(a) x-axis velocity. (b) z-axis velocity. (c) z-axis contact force.

Fig. 5: The comparison between the heel strike and the flat foot walking. The flat obstacle varied by a z-axis of 1cm is installed in the foot pathway. $\dot{\boldsymbol{z}}_d, \dot{\boldsymbol{z}}_{d2}$ represent the desired trajectory of the flat foot and the heel strike. **FF** and **HS** represent the flat foot trajectory and the heel strike trajectory.

TABLE I: Design parameters and sets. Gain sets are chosen via the author's experience. $m_{i,d}, b_{i,d}, k_{i,d}$ are components of $\boldsymbol{M}_d, \boldsymbol{B}_d, \boldsymbol{K}_d$.

Design parameters	small gain	proposed gain	large gain
$m_{1,d}$	6.0	6.0	6.0
$m_{2,d}$	0.11	0.11	0.11
$m_{3,d}$	0.12	0.12	0.12
$b_{1,d}$	54	300	300
$b_{2,d}$	0.8	4.2	4.2
$b_{3,d}$	0.9	2.4	4.6
$k_{1,d}$	1340	1340	3730
$k_{2,d}$	1.8	11	11
$k_{3,d}$	1.9	5.4	12

initial contact, as shown in Fig. 5b, because the impulsive force of the **HS** is smaller than **FF** after the initial contact, as shown in Fig. 5c. In addition, **HS** shows smaller fluctuations after contact. The other axes have the same characteristics, so it is omitted.

To see the effect of post-impact strategy, several simulations are conducted with three-parameter sets: Gain sets are chosen via the author's experience as shown in Table I. All sets have equivalent m values, and small gain(SG) set & large gain(LG) set are minimum and maximum of k, b values. LG generates smaller position/velocity errors, as shown in Fig. 6a and Fig. 6b. In spite, LG causes larger CoM/ZMP errors, as shown in Fig. 6c and Fig. 6d. Besides, SG generates larger position/velocity errors but smaller CoM/ZMP errors. Hence, the control parameters have to be tuned properly because CoM/ZMP show opposite characteristics compared to the position/velocity. Through the results, it is noticed that the fast regulation of foot landing does not ensure the regulation of CoM/ZMP and CoM/ZMP error reduction is the critical part of the parameter design in landing control. With the characteristics, proper control with the proposed gain(PG) set is shown in Fig. 6e and Fig. 6f. Modified trajectories reduce the tracking error, so it improves the walking performance.

In addition, from Fig. 5 and Fig. 6, it is noticed that greater impulsive force generates instability in the system. Therefore, the heel strike walking is more robust against obstacles than the flat foot walking and generates more compliant landing stably. In some cases, heel strike walking can overcome the obstacle which is not overcome by flat foot walking because of the stable landing.

TABLE II: Algorithm validation for uneven terrain walking. Experiment 1 represents small varied terrain and experiment 2 represents critically varied terrain.

	Success ratio (%)	
	Experiment 1	Experiment 2
FF	10	0
HS	50	0
FF+HAC	100	80
HS+HAC	100	100

B. Complex uneven terrain walking analysis

To validate the control algorithm's robustness, complex uneven terrain is installed in the middle of the footpath, as shown in Fig. 1. Ten random terrains with small variation and critical variation are used. The complex terrain 1 has variations on z-axis position of $0 \sim 1.2cm$, $0 \sim 2^\circ$ on x- & y-axis orientation in the experiment 1. In addition, the complex terrain 2 has variations on z-axis position of $0 \sim 3cm$, $0 \sim 5^\circ$ on x- & y-axis orientation in the experiment 2. The complex terrain 1 is used to compare the walking performance with/without the algorithm and the complex terrain 2 is used to show the robustness of the control. **FF** walking, **HS** walking are tested with/without **HAC**, and results are presented in Table II. As expected from the previous sections, **HS** shows better performance compared to the **FF**. In addition, **HAC** improves control performance much even in the critically various terrain experiment. In the case of experiment 2, **FF** and **HS** failed to walk on critically varied uneven terrain without **HAC**. However, **FF+HAC** and **HS+HAC** show the improvement in the walking control performance on critical rough terrain.

One of the results in experiment 1 is presented in Fig. 7. In Fig. 7, the foot and ZMP trajectories generated by **FF** and **HS + HAC** are depicted on the x-y plane. The errors of foot trajectory occur by landing on uneven terrain. As expected, **FF** fails to overcome the unexpected landing, so a larger displacement error is generated at each landing, especially in the last step. In the other hand, **HS + HAC** improves the tracking performance and the landing performance significantly.

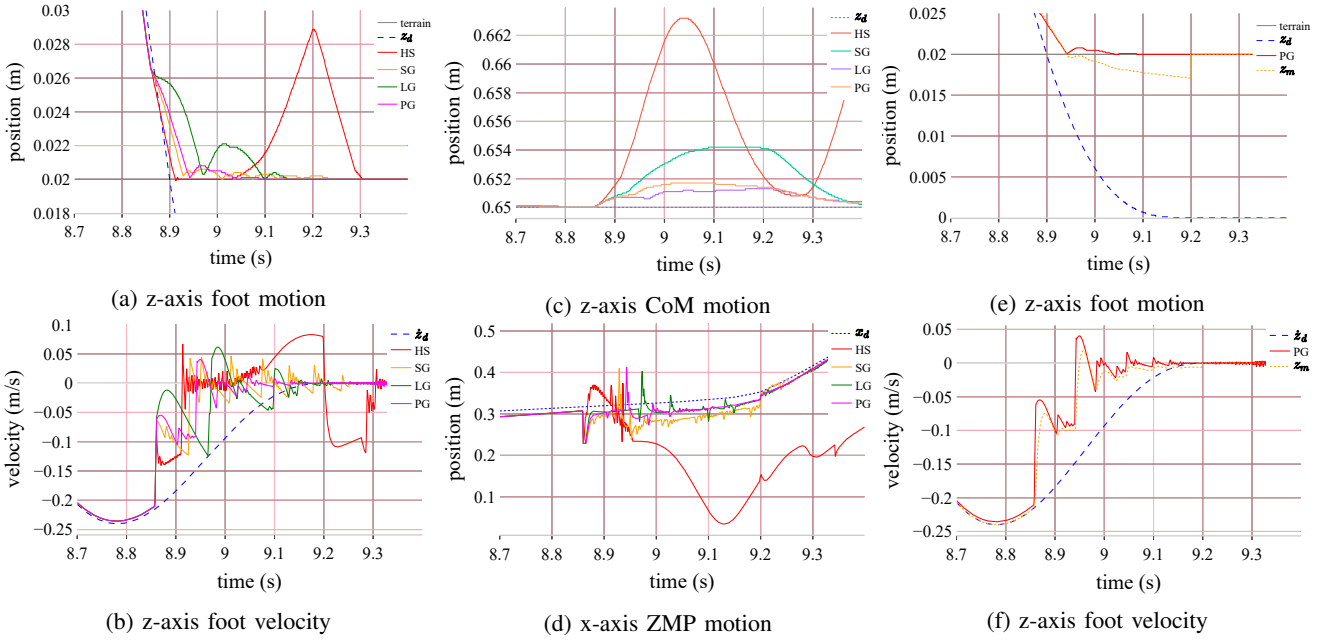

(a) z-axis foot motion (c) z-axis CoM motion (e) z-axis foot motion

(b) z-axis foot velocity (d) x-axis ZMP motion (f) z-axis foot velocity

Fig. 6: Motion comparison concerning the control parameter. The contact is occurred at $8.82s$. The dashed line is the desired trajectory, and the solid line is the z-axis trajectory of the foot. Besides, The dotted line is the modified trajectory.

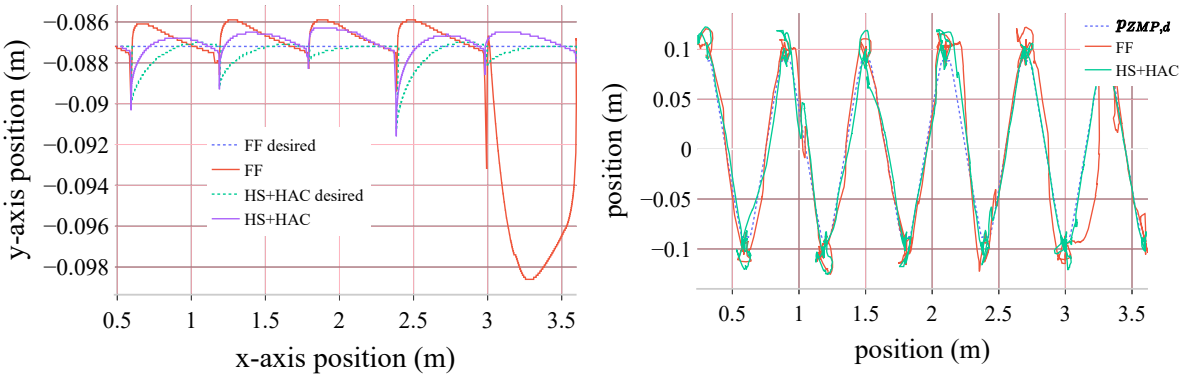

(a) Top view of foot trajectory. (b) Top view of ZMP trajectory.

Fig. 7: Top view of foot & ZMP trajectory using **FF** and **HS+HAC**.

VI. Conclusion

This paper proposed a robust landing stabilization of humanoid on uneven terrain. Humanoid walking with heel strike motion is conducted in the momentum-based whole-body control framework to find the robot configuration resulting in small impulsive force. Additionally, combining the admittance control (for landing related axes) with reset of post-contact reference (for slip related axes), **HAC** is employed to adjust post-contact reference of the swing foot on the contact terrain. The effect of heel strike walking in uneven terrain locomotion concerning the impulsive force is analyzed. Besides, the control parameters are carefully selected by considering the tracking performance of not only swing foot but also CoM and ZMP, because only a fast regulation of swing foot may not imply landing stabilization as the CoM and ZMP are largely perturbed.

Thus, we perform validation of the proposed algorithms via simulation. It was observed in the simulation that employing both **HS** and **HAC** leads to a significant improvement of the landing stability when the robot walks on uneven terrain.

References

[1] Y. Kim, B. Lee, J. Ryu and J. Kim, "Landing force control for humanoid robot by time-domain passivity approach," in *IEEE Transactions on Robotics*, vol. 23, no. 6, pp. 1294-1301, December 2007.

[2] J. Kim, I. Park, and J. Oh, "Walking control algorithm of biped humanoid robot on uneven and inclined floor," in *Journal of Intelligent and Robotic Systems*, vol. 48, no. 4. pp. 457-484, April 2007.

[3] S. M. Yoo, S. W. Hwang, D. H. Kim and J. H. Park, "Biped robot walking on uneven terrain using impedance control and terrain recognition algorithm," *2018 IEEE-RAS 18th International Conference on Humanoid Robots (Humanoids)*, Beijing, China, 2018, pp. 293-298.

[4] W. Xu, R. Xiong and J. Wu, "Force/torque-based compliance control for humanoid robot to compensate the landing impact force," *2010 First International Conference on Networking and Distributed Computing*, Hangzhou, 2010, pp. 336-340.

[5] J. H. Park and H. Chung, "Hybrid control for biped robots using impedance control and computed-torque control," *Proceedings 1999 IEEE International Conference on Robotics and Automation (Cat. No.99CH36288C)*, Detroit, MI, USA, 1999, pp. 1365-1370.

[6] Z. Li, N. G. Tsagarakis and D. G. Caldwell, "A passivity based admittance control for stabilizing the compliant humanoid COMAN," *2012 12th IEEE-RAS International Conference on Humanoid Robots (Humanoids 2012)*, Osaka, 2012, pp. 43-49.

[7] S. Caron, "Biped stabilization by linear feedback of the variable-Height inverted pendulum model," *2020 IEEE International Conference on Robotics and Automation (ICRA 2020)*, Paris, 2020.

[8] J. Jo and Y. Oh, "Impedance control of humanoid walking on uneven terrain with centroidal momentum dynamics using quadratic programming," *2020 IEEE/RSJ International Conference on Intelligent Robots and Systems (IROS 2020)*, Las Vegas, 2020.

[9] D. Torricelli, J. Gonzalez, M. Weckx, R. Jimenez-Fabian, B. Vanderborght, M. Sartori, S. Dosen, D. Farina, D. Lefeber D, and JL. Pons, "Human-like compliant locomotion: state of the art of robotic implementations," in *Bioinspiration & Biomimetics*, vol. 11, August 2016.

[10] S. Yi and D. D. Lee, "Dynamic heel-strike toe-off walking controller for full-size modular humanoid robots," *2016 IEEE-RAS 16th International Conference on Humanoid Robots (Humanoids)*, Cancun, 2016, pp. 395-400.

[11] M. Sadedel, A. Yousefi-Koma, M. Khadiv, and S. Mansouri, "Investigation on dynamic modeling of SURENA III humanoid robot with heel-Off and heel-Strike Motions," in *Iranian Journal of Science and Technology, Transactions of Mechanical Engineering*, vol. 41, no. 1, pp. 9?23, March 2017.

[12] S. Feng, "Online hierarchical optimization for humanoid control," Ph.D. dissertation, Carnegie Mellon University, 2016.

[13] T. Koolen, S. Bertrand, G. Thomas, T. De Boer, T. Wu, J. Smith, J. Englsberger, and J. E. Pratt, "Design of a momentum-based control framework and application to the humanoid robot atlas," in *International Journal of Humanoid Robotics*, vol. 13, March 2016.

[14] A. Herzog, N. Rotella, S. Mason, F. Grimminger, S. Schaal, and L. Righetti, "Momentum control with hierarchical inverse dynamics on a torque-controlled humanoid," in *Autonomous Robots*, vol. 40, no. 3, pp. 473?491, March 2016.

[15] M. Nikolić, B. Borovac, and M. Raković, "Dynamic balance preservation and prevention of sliding for humanoid robots in the presence of multiple spatial contacts," *Multibody System Dynamics*, vol. 42, pp. 197-218, April 2017.

[16] T. Luksch, "Human-like control of dynamically walking bipedal robots," Techniscen Universitat Kaiserslantern, 2010.

[17] S. Majid, A. Yousefi-Koma, F, Iranmanesh, "Analytical dynamic modelling of heel-off and toe-off motions for a 2D humanoid robot," in *Journal of Computational Applied Mechanics*, vol. 46, no. 2, pp. 243-256, January 2015.

[18] I. D. Walker, "The use of kinematic redundancy in reducing impact and contact effects in manipulation," in *Proceedings of IEEE International Conference on Robotics and Automation*, Cincinnati, OH, USA, 1990, pp. 434-439.

[19] Z. C. Lin, R. V. Patel, and C. A. Balafoutis, "Impact reduction for redundant manipulators using augmented impedance control," in *Journal of Robotic Systems*, vol. 12, no. 5, pp. 301-313, 1995.

[20] E. Todorov, T. Erez and Y. Tassa, "MuJoCo: A physics engine for model-based control," *2012 IEEE/RSJ International Conference on Intelligent Robots and Systems*, Vilamoura, 2012, pp. 5026-5033.